



ELSEVIER

Available online at www.sciencedirect.com

SCIENCE @ DIRECT®

Physica B 338 (2003) 284–290

PHYSICA B

www.elsevier.com/locate/physb

Modeled effects on permittivity measurements of water content in high surface area porous media

Scott B. Jones^{a,*}, Dani Or^b

^aDepartment of Plants, Soils, and Biometeorology, Utah State University, Logan, UT 84322-4820, USA

^bDepartment of Civil and Environmental Engineering, University Of Connecticut, Storrs, CT 06269-2037, USA

Abstract

Time domain reflectometry (TDR) has become an important measurement technique for determination of porous media water content and electrical conductivity due to its accuracy, fast response and automation capability. Water content is inferred from the measured bulk dielectric constant based on travel time analysis along simple transmission lines. TDR measurements in low surface area porous media accurately describe water content using an empirical relationship. Measurement discrepancies arise from dominating influences such as bound water due to high surface area, extreme aspect ratio particles or atypical water phase configuration. Our objectives were to highlight primary factors affecting dielectric permittivity measurements for water content determination in porous mixtures, and demonstrate the influence of these factors on mixture permittivity as predicted by a three-phase dielectric mixture model. Modeled results considering water binding, higher porosity, constituent geometry or phase configuration suggest any of these effects individually are capable of causing permittivity reduction, though all likely contribute in high surface area porous media.

© 2003 Elsevier B.V. All rights reserved.

Keywords: TDR; Dielectric; Mixing model; Bound water

1. Introduction

Time domain reflectometry (TDR) is a relatively new method for measurement of porous media water content and electrical conductivity [1]. Both of these attributes have substantial utility in studying a variety of hydrologic processes [2]. The first application of TDR to soil water measurements was reported by Topp et al. [3]. The main advantages of TDR over other soil water content measurement methods are: (i) superior accuracy to within 1% or 2% volumetric

water content; (ii) minimal calibration requirements – in many cases specific calibration is not needed; and (iii) TDR has excellent spatial and temporal resolution. The method's popularity is increasing and is capable of providing continuous measurements through automation and multiplexing. As the technology matures research interests turn more to the fundamental processes influencing the permittivity measurement. Along these lines, modeling of the dielectric permittivity using 1st principles facilitates improved understanding and future accounting and calibration of factors affecting measurements.

The dielectric constant of a material describes its ability to store electrical potential energy in

*Corresponding author. Fax: 435-755-8419.

E-mail address: scott.jones@usu.edu (S.B. Jones).

response to an applied electric field. The large contrast between the dielectric constant of water (~ 80) and that of air (1) and soil minerals (~ 5) yields highly accurate determinations of water content in a wide range of porous media. Fig. 1 illustrates several probe configurations showing the associated electric field lines. The Topp et al. [3] empirical relationship is widely used to describe the bulk dielectric (ϵ_b)–volumetric water content (θ) relationship (either $\epsilon_b(\theta)$ or $\theta(\epsilon_b)$) of a wide variety of porous media (Fig. 1), written as

$$\epsilon_b = 3.03 + 9.3\theta + 146\theta^2 - 76.7\theta^3. \quad (1)$$

Topp's relationship describes the measured dielectric of most agricultural and mineral soils with specific surface area, A_s , of less than $100 \text{ m}^2 \text{ g}^{-1}$ [4]. The two clay minerals Attapulgite and Bentonite shown in Fig. 1 exhibit A_s values of 270 and $665 \text{ m}^2 \text{ g}^{-1}$, respectively, and both clay particles are non-spherical. An empirical model fitted to high surface area porous media [5] better describes their permittivities. Moreover, the Bentonite clay shows an unusual and unique large increase in permittivity at mid-level water contents that neither curve describes. This behavior might be

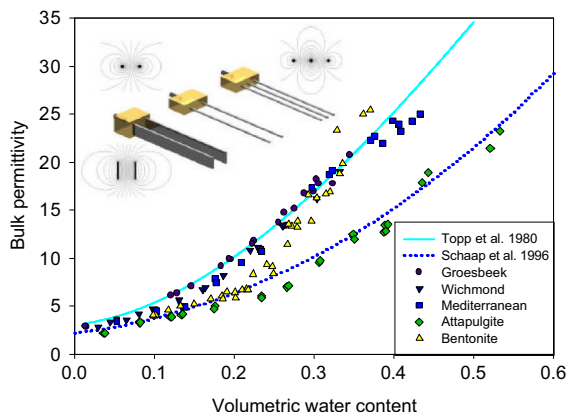


Fig. 1. Illustration of three different TDR probe configurations with their associated electrical field lines plotted in a cross-section of the probe geometry. A 3-rod TDR probe was used to measure the bulk permittivities for the five soils shown [4]. The Topp et al. [3] equation is the solid line representing the ϵ_b – θ relationship of mineral soils. Attapulgite and Bentonite are high surface area clays and correspond with the dotted line [5] representing permittivities of high surface area forest floor litter.

attributed to changes in porous medium water organization or phase configuration.

2. Measurement theory

Travel time analysis provides a measure of the apparent length (L_a) of the TDR probe embedded in the porous medium and relates the ratio of apparent to true length (L) with the soil's bulk dielectric constant (ϵ_b). The dielectric of the porous medium surrounding a probe influences signal propagation velocity ($v = 2L/t$) according to

$$\epsilon_b = \left(\frac{L_a}{L}\right)^2 = \left(\frac{ct}{2L}\right)^2, \quad (2)$$

where c is the speed of light in free space ($3 \times 10^8 \text{ m s}^{-1}$), and t is the reflected signal travel time (down and back = $2L$) along the TDR probe. Electrical conductivity is measured from the waveform amplitude at long times approximating DC behavior.

In the following we discuss factors affecting TDR measurement of permittivity in high surface area porous media and present a dielectric mixing model to account for certain effects influencing bulk permittivity for water content determination.

3. Factors influencing TDR measurements of permittivity

3.1. Free water, bound water and temperature

The permanent dipole moment of free water molecule results in a high value of static (low frequency) permittivity which is well characterized both as a function of temperature [6] and frequency [7]. Bulk (free) water exhibits a decrease in relative permittivity from 87 to 77 for an increase in temperature of from 0°C to 30°C , in contrast, solid permittivities remain practically constant with temperature changes ($\epsilon_b \sim 5$). The large permittivity contrast between free water and solids and air diminishes when water molecules are rotationally hindered and their permittivity is reduced. Molecules within the vicinity of solid surfaces are subjected to interfacial forces that

constrain their rotation, consequently, their ability to fully respond to an alternating electric field diminishes. The permittivity of such “bound water” may be close to the permittivity of the solid constituents making the water practically ‘invisible’ to the TDR measurement [8]. High surface area porous media bind a substantial fraction of their water phase, resulting in reduced ϵ_b measurements as illustrated in Fig. 1 [4,5].

The difficulty in quantifying the amount of bound water in a given system stems from the unknown thickness of the affected (bound) layer. Several modeling approaches have been suggested for describing this relationship [8–10]. Or and Wraith [8] applied temperature perturbations to a variety of soils and water contents to study the behavior of bound water. They identified an interplay among two competing phenomena, the first is the well-documented reduction in the permittivity of free water with increasing temperature [6]. This effect is presented in Fig. 2(a) where the free water permittivity, ϵ_{fw} , at 5°C and 25°C is illustrated by a reduction in the water phase permittivity. The second phenomenon is the apparent ‘release’ of bound water from a lower to a higher rotational state, which occurs with increasing temperature. This bound water effect is illustrated in Fig. 2(a) by a reduction in the bound water layer thickness, t_{bw} with increasing temperature. Or and Wraith [8] developed a temperature-dependent model to describe this bound water layer thickness, t_{bw} (m), given as

$$t_{bw}(T) = \frac{a}{-d + T \ln(kT/8\pi^2 r^3 b f_{rel})}, \quad (3)$$

where the constants $a = 1621$ (Δ K), $d = 2.047 \times 10^3$ (K), $b = 9.5 \times 10^{-7}$ (Pa s), k is the Boltzman constant (1.38062×10^{-23} (J K⁻¹)) and r (m) is the radius of the bound water molecule (~ 1.8 – 2.5 Å). This expression is based on an exponential viscosity profile of water near solid surfaces coupled with the Debye (1929) model predicting the relaxation frequency, f_{rel} (Hz), below which bound water relaxes. For standard TDR applications, a value for $f_{rel} = 1$ GHz was used by Or and Wraith [8].

The total water phase “layer” thickness, t_w (m), may be expressed in terms of the volumetric water

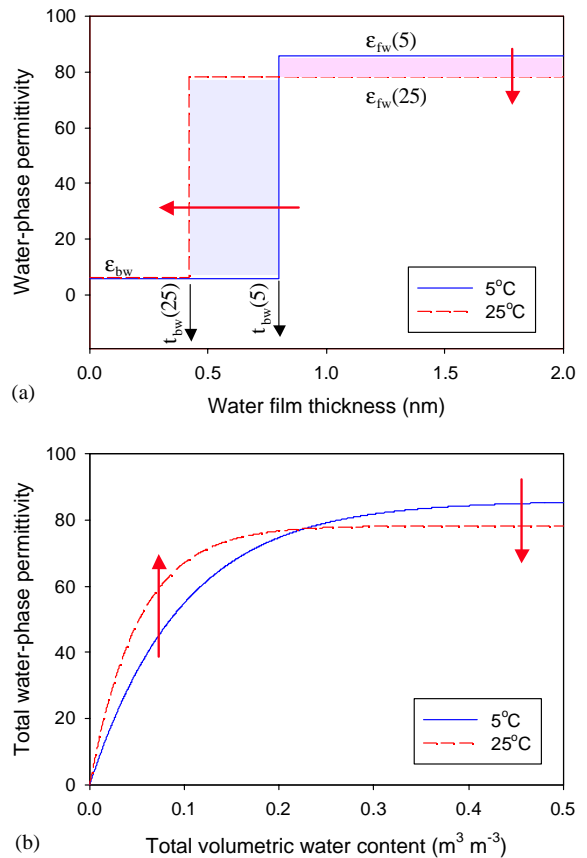


Fig. 2. Illustration of the thermodielectric effect described by the temperature-dependent responses of the free water phase permittivity (ϵ_{fw}) and the bound water layer thickness (t_{bw}). In (a) the temperature increase from 5°C to 25°C is described by the reduction of t_{bw} releasing bound water to a more rotational state, which results in a higher effective permittivity. The free water permittivity is reduced with increasing temperature. In (b) these competing phenomena are illustrated as the total water phase permittivity plotted using Eq. (4) and demonstrating the thermodielectric behavior as a function of water content.

content, θ_v , the porous medium bulk density, ρ_b ($Mg\ m^{-3}$), and specific surface area, A_s ($m^2\ kg^{-1}$), where $t_w = \theta_v / (A_s \rho_b)$. Jones and Or [11] expressed the temperature dependent total water phase permittivity by

$$\epsilon_w(T) = \epsilon_{fw}(T) \left(1 - \exp \left(\frac{-(\theta_v / A_s \rho_b)}{t_{bw}(T)} \right) \right). \quad (4)$$

Fig. 2(b) illustrates the modeled temperature dependent permittivity described by Eq. (4). The

main attributes that determine the direction and magnitude of the combined temperature effect appear to be the average water content and specific surface area of the porous medium; both determine the ratio of bulk to bound water in the system and hence the relative importance of these competing processes.

3.2. Particle shape anisotropy

The permittivity measurement in porous media is influenced by constituents comprising the mixture due to the alteration in the electric field imposed by the particle size and geometry. The geometrical descriptor convenient for modeling particle shape is termed the depolarization factor, N [12], which is often assumed an ellipsoidal or spheroidal geometry defining the particle shape in terms of its axial aspect ratio where the rotation axis, a , is divided by the common axes, b or c , assuming a spheroidal geometry (see inset of Fig. 3). Aligned particles impart the greatest ‘geometrical’ influence on the measured permittivity, which can either enhance or diminish the permittivity relative to measurements in a random mixture of the same particles with a fixed packing density (assuming this were possible). Jones and

Friedman [13] presented the following empirical expression describing the depolarization factor as a function of spheroid aspect ratio:

$$N_p = \frac{1}{1 + 1.6(a/b) + 0.4(a/b)^2}, \quad N_n = \frac{1 - N_a}{2}, \quad (5)$$

where N_p and N_n are the depolarization factors when the electric field is aligned parallel and normal to the axis of rotation, respectively. These relationships are plotted in Fig. 3 as a function of aspect ratio for extreme shapes from oblate to prolate. The maximum depolarization (e.g., leading to permittivity reduction) occurs for oblate particles having the electric field aligned parallel to their rotation axis (e.g., $N_p = 1$). The polarizing influence of thin disks or long needles is maximized when the electric field runs normal and parallel to their rotation axis, respectively (e.g., $N_p = N_n = 0$).

3.3. Constituent phase configuration

For the three-phase confocal ellipsoid depicted in Fig. 3, the core, ϵ_2 , and the outer shell, ϵ_1 , are contained in a background host medium of permittivity, ϵ_0 . For such a system, six different phase configurations are possible for solid (S) water (W) and air (A) phases (i.e., SWA, SAW, ASW, AWS, WSA, WAS). Friedman [9] employed concentric spheres in a combination of SWA and ASW phase configurations to model the water content (via permittivity) of 22 porous media. The modeled results were generally well correlated to data using an effective medium approximation of the combined phase configurations weighted based on water content (e.g., dry = SWA, saturated = ASW). A similar approach using combinations of WSA (drier) and SWA (wetter) was well suited to describe the lower permittivities of moist cereal grains where water is deeply embedded within the kernel’s hierarchical structure [9].

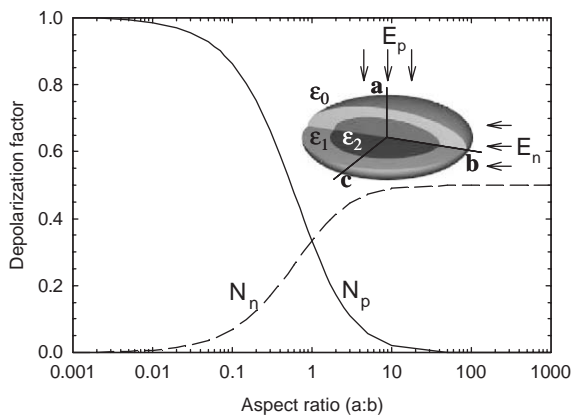


Fig. 3. Depolarization factor, N , as a function of aspect ratio, a/b , and electric field (E) alignment (i.e., normal, n, or parallel, p) with respect to the spheroid axis of rotation, a (e.g., E_p describes an E -field aligned parallel to (a)). The ellipsoid contains a core, ϵ_2 , and concentric shell, ϵ_1 , lying in a background, ϵ_0 , representing a three-phase dielectric medium.

4. Three-phase dielectric mixture model

The confocal ellipsoid model shown in Fig. 3 contains water, solid and air phase permittivities

labeled $\epsilon_w, \epsilon_a, \epsilon_s$ and their respective volumetric fractions are ϕ_w, ϕ_a , and ϕ_s . The bound and free water phase permittivities are modeled as a continuous phase using Eq. (4). The air and solid phases are assigned values of $\epsilon_a = 1$ and $\epsilon_s = 5$ [14]. Constituent volume fractions are related using measurable quantities of bulk density (ρ_b) and particle density (ρ_s) from which we obtain bulk porosity (ϕ_b) (i.e., $\phi_b = 1 - \rho_b/\rho_s$). The air (ϕ_a) and solid (ϕ_s) fractions may be written as $\phi_a = \phi_b - \phi_w$ and $\phi_s = 1 - \phi_b$, respectively.

A multi-phase ellipsoid model allows for accounting of particle shape effects via the depolarization factor (Eq. (5)) in addition to phase configuration effects. The effective permittivity of such a system was modeled based on the Maxwell-Garnett theory [15] by Sihvola and Lindell [16] for any number of ellipsoid shells, written as

$$\epsilon_b = \epsilon_0 + \frac{(\epsilon_0/3) \sum_{i=p,n,n} (n_v \alpha^i / \epsilon_0)}{1 - \frac{1}{3} \sum_{i=p,n,n} N_1^i (n_v \alpha^i / \epsilon_0)}, \tag{6}$$

where i refers to any of three possible electric field orientations with respect to the rotation axis (i.e., in Fig. 3 inset, parallel, normal or normal) and the polarizability term in parenthesis is given as a series expansion, written here as

$$\frac{n_v \alpha^i}{\epsilon_0} = (\phi_1 + \phi_2) \frac{\left\{ (\epsilon_1 + \epsilon_0) + [\epsilon_1 + N_1^i(\epsilon_0 - \epsilon_1)] \frac{\epsilon_2 - \epsilon_1 \frac{\phi_2}{(\phi_1 + \phi_2)}}{[\epsilon_1 + N_2^i(\epsilon_2 - \epsilon_1)]} \right\}}{\left\{ [\epsilon_0 + N_1^i(\epsilon_1 - \epsilon_0)] + N_1^i(1 - N_1^i)(\epsilon_1 - \epsilon_0) \frac{(\epsilon_2 - \epsilon_1) \frac{\phi_2}{\phi_1 + \phi_2}}{\epsilon_1 + N_2^i(\epsilon_2 - \epsilon_1)} \right\}} \tag{7}$$

where ϕ_1 and ϕ_2 are the volumetric fractions and N_1^i and N_2^i are the depolarization factors of the shell and core ellipsoids, respectively.

4.1. Modeled results

A number of the factors affecting permittivity measurements may be approximated using Eqs. (6) and (7). The importance of such an approximation

is underlined by the difficulty in actually isolating and measuring some of these individual effects experimentally. An example is the case of plate-like clay particles that exhibit extreme aspect ratio, high porosity and large specific surface area. Modeling these effects provides some sense of the expected influence on the measurement of permittivity within the limited context of the mixing theory. Fig. 4 shows a comparison of computed permittivities using Eqs. (6) and (7) as a function of volumetric water content. For each effect modeled a common set of parameters is used unless otherwise specified, which includes a phase configuration of solid–water–air (SWA), a bulk porosity (ϕ_b) of 0.5, a specific surface area (A_s) of $100 \text{ m}^2 \text{ g}^{-1}$, and an aspect ratio (a/b) of 1. The Topp et al. equation (Eq. (1)) is also shown for comparison.

The influence of specific surface area on the water phase permittivity (Eq. (4)) is illustrated in Fig. 4(a) where greater surface area results in greater water binding leading to a decrease in ϵ_b . These predictions follow the trend for higher surface area clays of Attapulgite and Bentonite (at low water content) shown in Fig. 1. The jump in permittivity in the Bentonite is not clearly understood, but is complicated by the swelling

nature of this clay, whose expansion increases the porosity with added water and thereby altering the water layer thickness between platelets.

Fig. 4(b) illustrates the influence of particle shape comparing spherical, oblate and prolate shapes, which for the SWA configuration shows an increased permittivity for both oblate and prolate shapes compared to spherical particles. It should be pointed out that this shape effect is also

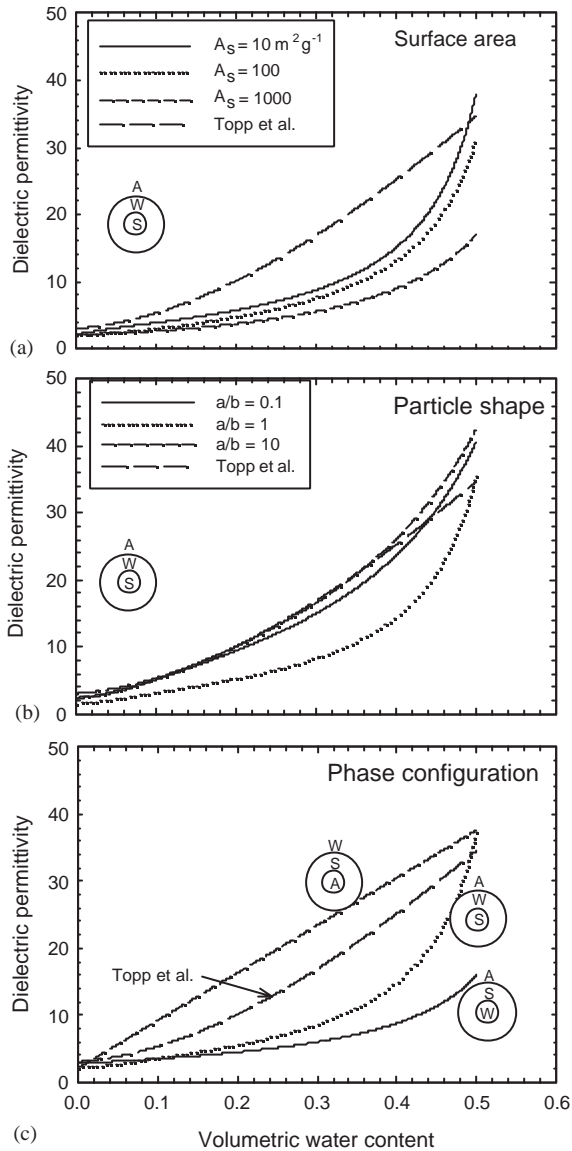


Fig. 4. Isotropic mixture permittivities modeled (Eqs. (6) and (7)) considering different factors: (a) specific surface area (bound water), (b) particle shape (aspect ratio, a/b), and (c) phase configuration. Default values used were $\phi_b = 0.5$, $A_s = 100 \text{ m}^2 \text{ g}^{-1}$, $a/b = 1$, and a SWA configuration. Variations are as specified in the figure.

phase configuration-dependent and exhibits an opposite effect (spherical shape exhibits highest permittivity) when comparing an ASW configuration for example [13].

The effect of phase configuration on permittivity is illustrated using default parameters for each of the three configurations shown in Fig. 4(a). The influence of different phase configurations on the predicted permittivity is dominated by the location of the water phase. For the case when water forms the background phase, the permittivity increase with water content is practically linear, while when water forms the ‘core’ phase (i.e., WSA) there is only a marginal increase in permittivity in comparison to the other two phases. The analogy of water buried within the solid (e.g., clay aggregates) is similar to a WSA phase configuration.

5. Summary

TDR measurements are routinely used to provide information on water content and salinity levels in porous media. In most low surface area media where water content is the dominant factor influencing the permittivity the Topp et al. empirical relation adequately describes this relationship. For porous media with high surface area and complex structured geometry, secondary effects often complicate the interpretation of water content from the permittivity reading. The intermingled effects of bound water, particle shape, phase configuration and porosity may influence the resulting permittivity measurably based on a three-phase dielectric mixture model. Surprisingly, phase configuration may be among the most significant, rivaling effects due to bound water. Improved measurement techniques are needed to isolate or eliminate these confounding factors for improved interpretation of the permittivity–water content relationship in high surface area porous media.

Acknowledgements

Partial funding was provided by a USDA-NRI competitive grant No. 2002-35107-12507. We gratefully acknowledge research grants from Campbell Scientific and Harvestmaster (Logan, Utah, USA) and from Pioneer Hi-Bred International (Johnston, IA, USA).

References

- [1] K. Noborio, *Comput. Electron. Agric.* 31 (2001) 213.
- [2] S.B. Jones, J.M. Wraith, *D. Or, Hydrol. Proces.* 16 (2002) 141.
- [3] G.C. Topp, J.L. Davis, A.P. Annan, *Water Resour. Res.* 16 (1980) 574.
- [4] C. Dirksen, S. Dasberg, *Soil Sci. Soc. Am. J.* 57 (1993) 660.
- [5] M.G. Schaap, L. deLange, T.J. Heimovaara, *Soil Technol.* 11 (1996) 205.
- [6] R.C. Weast, *CRC Handbook of Chemistry and Physics*, CRC Press, Boca Raton, FL, 1986.
- [7] U. Kaatze, in: A. Kraszewski (Ed.), *Microwave Aquametry*, IEEE Press, New York, 1996, p. 37.
- [8] D. Or, J.M. Wraith, *Water Resour. Res.* 35 (1999) 371.
- [9] S.P. Friedman, *Water Resour. Res.* 34 (1998) 2949.
- [10] D.A. Robinson, J.D. Cooper, C.M.K. Gardner, *J. Hydrol.* 255 (2002) 39.
- [11] S.B. Jones, D. Or, in: K. Kupfer, C. Hubner (Eds.), *Fourth International Conference on Electromagnetic Wave Interactions with Water and Moist Substances*, MFPA an der Bauhaus-University of Weimar, Weimar Germany, 2001, p. 46.
- [12] L.D. Landau, E.M. Lifshitz, *Electrodynamics of Continuous Media*, Pergamon Press, New York, 1960.
- [13] S.B. Jones, S.P. Friedman, *Water Resour. Res.* 36 (2000) 2821.
- [14] S. Dasberg, F.N. Dalton, *Soil Sci. Soc. Am. J.* 49 (1985) 293.
- [15] J.C. Maxwell-Garnett, *Trans. Roy. Soc. (London) Serial A* 203 (1904) 385.
- [16] A. Sihvola, I.V. Lindell, *J. Electromagn. Waves Appl.* 4 (1990) 1.